Available online at www.sciencedirect.com
ScienceDirect
Journal of the European Ceramic Society 31 (2011) 559–568
www.elsevier.com/locate/jeurceramsoc

Correlation between microstructure and electrical conductivity in composite electrolytes containing Gd-doped ceria and Gd-doped barium cerate

Mudrika Khandelwal, A. Venkatasubramanian, T.R.S. Prasanna, P. Gopalan *

Department of Metallurgical Engineering and Materials Science, Indian Institute of Technology Bombay, Powai, Mumbai 400 076, India

Received 10 December 2009; received in revised form 14 October 2010; accepted 27 October 2010
Available online 8 December 2010

Abstract

Composite electrolytes with nominal compositions, $Ce_{0.8}Gd_{0.2}O_{1.9} + xBaO$ ($x = 0.2$ and 0.3), have been synthesized through the citrate route. Formation of two phases, namely Gd-doped ceria and Gd-doped barium cerate, has been confirmed through XRD and SEM studies. The impedance spectra show three distinct semi-circles, all originating from the composite electrolytes. In the temperature range 175–350 °C, the activation energies for the conductivity values extracted from the high frequency and intermediate frequency parts of the impedance spectra remains the same, irrespective of compositional and micro-structural variation. On the other hand, the activation energies for the conductivity values associated with the low frequency impedance spectra show a significant change with micro-structural variation. Solid oxide fuel cells constructed using these composite electrolytes exhibit a higher open circuit voltage compared to those based on single phase 20 mol% Gd-doped ceria.

Keywords: Composite; Ceria; Impedance spectroscopy; Electrical conductivity; Fuel cell

1. Introduction

Solid oxide fuel cells (SOFC) hold a clean, efficient and promising solution for the ever-increasing demands for energy. The electrolyte is one of the key components, which decide the performance of a SOFC. Currently, commercially available SOFCs, using yttria-stabilized zirconia (YSZ) as an electrolyte, have to operate around 1000 °C to meet the required performance characteristics. This is essentially because the total conductivity of YSZ based electrolyte reaches the required value 0.1 S cm^{-1}, only at this temperature.[1] But, such a high operating temperature causes reactions between various components of a SOFC and, thus, limits the choice of materials for the other components. Hence, lowering the operating temperature would widen the range of materials useful in various components of a SOFC. In addition, the lower operating temperatures would also facilitate a faster start up and shut down of a SOFC system.

The doped-ceria based electrolytes are noteworthy candidates for reducing the operating temperature, as they exhibit the required conductivity 0.1 S cm^{-1} at 800 °C.[2] Introduction of aliovalent cations, like Gd^{+3}, into the host lattice of CeO_2 increases the concentration of oxygen vacancies (as shown by Eq. (1)) and results in improved conductivity.

$$Gd_2O_3 \rightarrow 2Gd'_{Ce} + V_o^{\bullet\bullet} + 3O_o^x \quad (1)$$

However, Gd-doped ceria, under reducing conditions at anode, invoke leakage current in the form of electronic conductivity, and thus diminish the cell output in terms of open circuit voltage (OCV).[3]

Another class of electrolytes based on doped-barium cerate exhibits proton and oxygen ion conductivity, depending on atmosphere and temperature.[4] Introduction of trivalent dopants like Gd^{+3} into barium cerate ($BaCeO_3$) results in the formation of oxygen vacancies, subsequently these vacancies react with H_2O (moisture) present in ambient air to form defects capable of proton conduction, in addition to the oxygen ion conductivity, as described below in Eqs. (2) and (3).

$$2Ce_{Ce}^x + O_o^x + Gd_2O_3 \rightarrow 2Gd'_{Ce} + V_o^{\bullet\bullet} + 2CeO_2 \quad (2)$$

$$H_2O + V_o^{\bullet\bullet} + O_o^x \leftrightarrow 2OH_o^{\bullet} \quad (3)$$

Moreover, $BaCeO_3$ based materials are resistant to the electronic leakage conduction.[5] Thus, if a composite electrolyte is made from the combination of doped-ceria and doped-barium

* Corresponding author. Tel.: +91 22 25767635; fax: +91 22 25722545.
E-mail address: pgopalan@iitb.ac.in (P. Gopalan).

0955-2219/$ – see front matter © 2010 Elsevier Ltd. All rights reserved.
doi:10.1016/j.jeurceramsoc.2010.10.027

cerate, it is expected that the doped-barium cerate phase can act as a blocking phase to the leakage current generated by the reduction of the doped-ceria phase. This should increase the OCV of the fuel cell as compared to those employing doped-ceria based electrolyte. Furthermore, these composites would have the advantage of additional proton conductivity displayed by the doped-barium cerate phase. Hirabayashi et al.[6] obtained higher OCV by growing a layer of $BaCe_xSm_{(1-x)}O_{3-\delta}$ on $Ce_{0.8}Sm_{0.2}O_{1.9}$ than $Ce_{0.8}Sm_{0.2}O_{1.9}$ alone as an electrolyte. Zhu et al.[7] have also reported improvement in OCV for a composite of $BaCe_{0.8}Y_{0.2}O_{2.9}$ and $Ce_{0.8}Sm_{0.2}O_{1.9}$ over only doped-ceria based electrolyte.

Understanding the correlation between microstructure and electrical behavior of composites of doped ceria and doped barium cerate is important from, both, fundamental and application point of view. The impedance spectroscopy has been widely used to characterize the electrical behavior of single phase doped-ceria as well as doped-barium cerate systems.[8–11] Impedance spectroscopy has been helpful to separate the grain and grain boundary impedance contributions to the total impedance of the electrolyte. The electrical behavior of YSZ/Al_2O_3, YSZ/MgO, YSZ/Y_2O_3 and $Ce_{0.8}Gd_{0.2}O_{2-\delta}/Al_2O_3$ composites, as electrolyte, has been studied in detail using impedance spectroscopy.[12–15] Moreover, the analysis of the impedance spectra can give meaningful insights into many aspects of the composite conductivity like percolation threshold of the second phase and blocking effect produced by the lower conducting phase.[12,13,16] To our knowledge, no detailed impedance spectroscopy studies have been done to understand the correlation between microstructure and electrical behavior of doped ceria and doped barium cerate composite systems; an attempt has thus been made in the current work.

Composites of Gd-doped ceria and Gd-doped barium cerate have been synthesized through the citrate (modified Pechini) route as reported in the literature.[17,18] The advantages of this wet chemical route over conventional solid state synthesis methods have been reported in terms of lower calcination temperatures, lower activation energy for the grain boundary conductivity and higher total conductivity obtained for wet chemical route.[19,20] The variation in microstructure has been obtained by varying the sintering temperature. The effect of these different microstructures on the electrical properties of the composite has been studied by impedance spectroscopy. The utility of these samples as an electrolyte for a SOFC has also been evaluated.

2. Experimental details

2.1. Powder preparation

Composites of Gd-doped ceria (CG) and Gd-doped barium cerate (BCG) with nominal molar ratio of 8:2 (B20CG) and 7:3 (B30CG), along with the compounds 20 mol% Gd-doped ceria (CG20) and 15 mol% Gd-doped barium cerate (BCG15), were synthesized through the citrate process. Barium carbonate ($BaCO_3$, 99.99%, Alpha Aesar), gadolinia (Gd_2O_3, 99.99%, Alpha Aesar), cerium nitrate hexahydrate ($Ce(NO_3)_3{\cdot}6H_2O$, 99% Aldrich) were used as the starting material for the synthesis. Citric acid (CA) ($C_6H_8O_7$, Merck, 99%) and ethylene glycol (EG) ($C_2H_6O_2$, Merck, 99%) were used as a chelating agent and reaction medium, respectively. The Gd_2O_3 was dissolved in dilute nitric acid to obtain a clear solution with constant stirring. $Ce(NO_3)_3{\cdot}6H_2O$ and $BaCO_3$ (except for CG20) were added to the solution subsequently. The molar ratio of EG/CA/metal ion was fixed as 20:5:1.[17] The resulting solution was dried in an oven at 80 °C to promote gelation. The gel obtained was heated at 300 °C for 4 h to obtain polymeric precursor. The CG20 precursor was calcined at 600 °C for 2 h, while others were calcined at 1100 °C for 4 h to obtain the required phases. Powders were ball milled in polyethylene terephthalate containers with ethyl alcohol for 48 h to reduce the particle size. The yttria stabilized zirconia balls were used as a grinding medium. The particle size analysis was performed on Galai CIS-I and sodium pyrophosphate was used as a dispersant.

2.2. Pellet fabrication

Pellets of thickness ranging between 1.1 and 2.6 mm were made by uni-axial compression in a steel die of diameter 10 mm with a pressure of 100 MPa. The pellets fabricated from CG20, BCG15, B20CG and B30CG were sintered at 1550 °C for 10 h on an alumina plate, referred now on as CG201550, BCG151550, B20CG1550 and B30CG1550, respectively. Pellets from the CG20, BCG15 and B20CG were also sintered at 1450 °C for 10 h and would be identified as CG201450, BCG151450 and B20CG1450 in the further discussion. The heating rate was maintained at 2 °C min^{-1} in the process of sintering. The surface of the pellet in contact with the alumina plate was polished with SiC paper (600 grit) to remove any reaction products.

2.3. Phase analysis

X-ray diffraction (XRD) studies were carried out on powders in a PANanalytical PW3040/60 X'pert PRO diffractometer (Cu K_α). A scanning rate of 10^{-3} degree s^{-1} was employed. Reitveld refinement of the XRD data was done using software (BRASS) to estimate the composition and the unit cell volume of the component phases in the composite samples.[21] The parameters for CeO_2 (fluorite *Fm3m*) and $BaCeO_3$ (orthorhombic *Pmcn*) were used as the starting structural models for refinement in the software.[22,23]

2.4. Microstructural analysis

The pellets were polished with an emery paper, diamond paste and colloidal silica for scanning electron microscopy (SEM) and energy dispersive spectroscopy (EDS) studies. Thermal etching was done at a temperature 100 °C lower than the sintering temperature of each pellet for 2 h. The SEM was performed on a Hitachi S3400N. The SEM images of all the composites were analyzed to find out the grain size distribution using Olysia m3 software (Olympus Corporation, Tokyo, Japan).[24] The backscattered images, from SEM, were processed using the software to improve the contrast for grain size analysis. For selecting the phases, manual as well automatic selection method was adopted.

Each phase was separately analyzed to obtain the grain size distribution in all the composites.

2.5. Electrical conductivity

A platinum coating (General Trading Corporation, Mumbai, India) was applied on both the surfaces of the pellet to serve as two electrodes. The platinum coated pellets were then fired at 1000 °C for 1 h to ensure good adhesion between the sample surface and platinum electrode. The impedance measurements were carried out as a function of frequency using a HP4192A impedance analyzer. A ProboStat™ sample holder (Norwegian Ceramic Society, Norway) was employed for all temperature dependent conductivity measurements in ambient air. The sample holder was placed in a vertical tube furnace to carry out the impedance measurements. A Eurotherm 2416 temperature controller monitored the heating and cooling rate of the furnace. The impedance measurements were carried out over the frequency range of 10^2–10^7 Hz and 20 measurements per decade of frequency were obtained. An applied potential of 1 V was used for the temperature range 100–600 °C, and 0.1 V for the temperature range 625–800 °C. As the electrolytes studied in the current work are expected to have a linear voltage–current relationship, relatively high voltage amplitude (1 V) was used at low temperatures to minimize noise in the impedance response.[25] The impedance values were collected during the cooling cycle. The impedance spectra were fitted to the conventional equivalent circuit containing resistance-constant phase element (R-CPE) sub circuits using the Zview software (Version 3.0, Scribner Associates, Inc.).[26] The circuit elements like inductor, warburg element were also used to account for the response of electrode to applied potential. The capacitance values were extracted using the formula:

$$C = Y^{(1/n)} R^{(1/n-1)} \quad (4)$$

where, R being resistance, Y and n being two parameters that characterize CPE used for fitting.

2.6. Fuel cell test

An apparatus was fabricated to measure the cell voltage as a function of current using the prepared composite electrolytes in form of a planar electrolyte supported SOFC. The thicknesses of CG201550, B20CG1550, B20CG1450 and B30CG1550 pellets were 1.7, 2.2, 2.3 and 2.5 mm, respectively. The pellets were coated with platinum paste over 3.5 mm diameter on both sides and fired at 1000 °C for 1 h, to serve as a cathode and anode. An alumina tube of inner and outer diameter 5 mm and 8 mm, respectively, was used as a support tube. A gold washer of 6 mm inner diameter and 8 mm outer diameter was employed as a sealant. A platinum mesh was used as a current collector for both the electrodes and platinum wires in contact with the current collector served as leads. The electrical contact and sealing were ensured by a spring loaded assembly. The entire setup was kept inside a vertical tube furnace. Humidified hydrogen was supplied at a flow rate 50 ml min^{-1} to the anode chamber and cathode was exposed to ambient air. The measurements were carried out using a Keithley 6221 current source and Keithley 2182A nanovoltmeter, during the cooling cycle in the temperature range 800–650 °C in steps of 50 °C. The peak marked SH originates from the sample holder used.

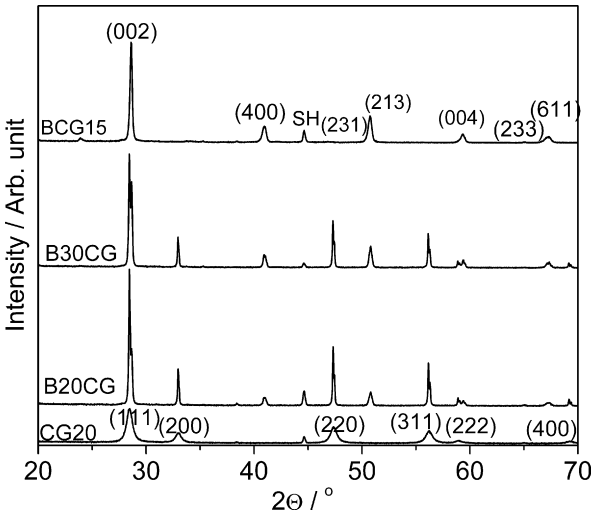

Fig. 1. Powder X-ray diffraction patterns of CG20, B20CG, B30CG and BCG15. The peak marked SH originates from the sample holder used.

3. Results and discussion

3.1. X-ray diffraction

The X-ray diffraction (XRD) patterns for the calcined powders CG20, BCG15, B20CG and B30CG are shown in Fig. 1. The XRD patterns of CG20 and BCG15 match with that of fluorite (JCPDS Reference code: 01-075-0162) and orthorhombic pervoskite structure (JCPDS Reference code: 01-082-2373), respectively. The XRD patterns of B20CG and B30CG clearly show presence of two different phases. One phase corresponds to Gd-doped ceria (CG) and the other phase to Gd-doped barium cerate (BCG). Table 1a lists the lattice parameters for all the phases present in the samples, extracted from the XRD data. In composite samples, the unit cell volume of CG phase is found to be higher than that of CG20. This can be attributed to the higher concentration of Gd in CeO_2 phase in composites as compared to single phase CG20.[27] On the contrary, a decrease in the BCG phase unit cell volume is seen, as compared to BCG15 unit cell volume.[28] This decrease in the cell volume may be due to less than 15 mol% of Gd occupying Ce site and/or partial occupation of Ba sites by Gd in $BaCeO_3$ as has been reported elsewhere.[29]

Table 1a
Lattice parameters and unit cell volumes extracted from the X-ray diffraction data.

Sample	CG phase		BCG phase			
	a/Å	V/Å^3	a/Å	b/Å	c/Å^3	V/Å^3
CG20	5.421	159.3				
B20CG	5.426	159.8	8.774	6.244	6.224	340.9
B30CG	5.428	159.9	8.777	6.241	6.223	340.8
BCG15			8.769	6.243	6.203	342.5

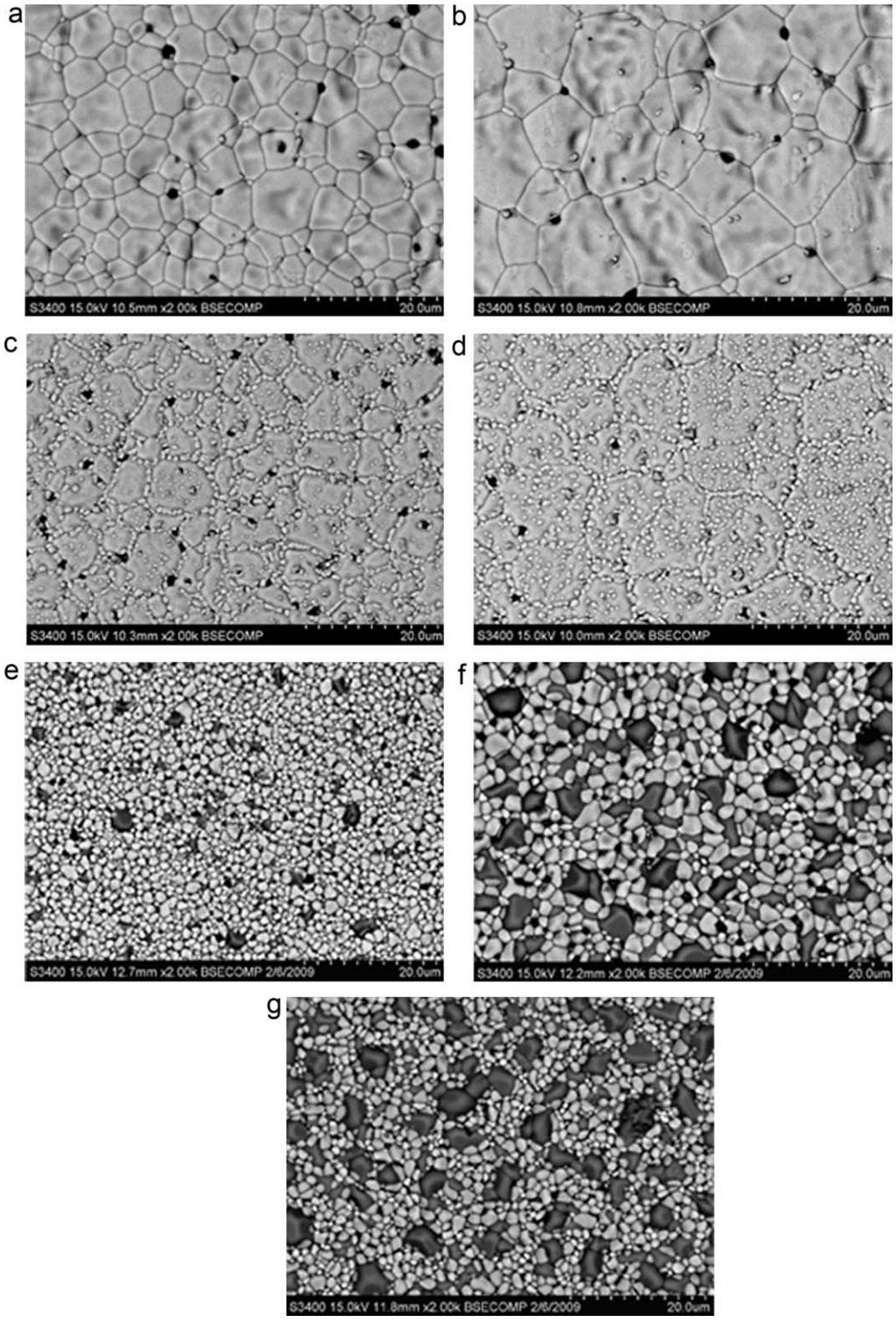

Fig. 2. Back scattered electron images of sintered surfaces of (a) CG201450, (b) CG201550, (c) BCG151450, (d) BCG151550, (e) B20CG1450, (f) B20CG1550 and (g) B30CG1450.

3.2. Particle size analysis

The powders of the two composites were analyzed to obtain mean particle size before and after ball milling. The mean particle size of B20CG decreased from 1.6 μm to 0.75 μm whereas that for B30CG decreased from 1.3 μm to 0.8 μm after ball milling. However, ball milling did not have much effect on the particles of CG20.

3.3. SEM

The back scattered electron (BSE) images of CG201450 and CG201550 are shown in Fig. 2(a) and (b), respectively. The mean grain sizes of CG201450 and CG201550 are 5.03(±1.74) μm and 11.29(±4.49) μm, respectively. The mean grain sizes of CG20 exhibit a slightly more than 2-times increase, on increasing the sintering temperature from 1450 °C to 1550 °C. This trend is consistent with the temperature dependent grain size obtained for CG20 by Christie et al.[8] The BSE images of BCG151450 and BCG151550 are shown in Fig. 2(c) and (d), respectively. The mean grain sizes of BCG151450 and BCG151550 are 6.77(±1.80) μm and 13.02(±3.28) μm, respectively. The mean grain size of BCG15 shows nearly 2-times increase, on increasing the sintering temperature from 1450 °C to 1550 °C. This observation is consistent with the grain growth seen with the increasing sintering temperature for BCG15 by Haile et al.[10] Furthermore, large mean grain size of samples CG201550 and BCG151550 implies relatively small contribution from the grain boundaries towards the total impedance.

Fig. 2(e)–(g) shows BSE images of the composite samples for B20CG1450, B20CG1550 and B30CG1550. These images reveal no porosities, thus avoiding any possible effect of these on the impedance response of the samples. The two contrasting phases are distinctly visible in each image. The elemental dispersive spectrum (EDS) indicated presence of Gd, Ce, O, Ba in the dark phase and Gd, Ce, O in the bright phase. This confirms that the dark phase corresponds to the BCG phase, while the bright phase is the CG phase. This observation of a two-phase microstructure is consistent with the two phase prediction by XRD.

The BSE images of B20CG1450 and B20CG1550 are shown in Fig. 2(e) and (f), respectively. A general increase in the grain size of each of BCG and CG phases has been observed with an increase in the sintering temperature of the samples. The mean grain sizes of CG phase in B20CG1450 and B20CG1550 are 0.85(±0.4) μm and 0.95(±0.8) μm respectively, while that of BCG phase in B20CG1450 and B20CG1550 are 1.25(±0.6) μm and 4.3(±2.0) μm, respectively. Thus, on increasing the sintering temperature from 1450 °C to 1550 °C, the mean grain size of CG phase experiences a very small increase, whereas the mean grain size of BCG phase at 1550 °C is almost 3-times that of at 1450 °C. The indicates that, with increase in sintering temperature, the grain growth of BCG phase in composite resembles the single phase BCG15, whereas that of CG phase does not; this is likely to be due to the pinning of CG grains by the presence and simultaneous growth of BCG grain.[15,16] In B30CG1550, the mean grain size of CG and BCG phase are 1.23(±1.02) μm and 3.79(±1.46) μm, respectively (Fig. 2(g)). Thus, increasing the mole fraction of BCG phase from 20% to 30% in the composite system did not show a significant change in the grain size of individual phases.

The microstructures of composites do not show percolation clearly (Fig. 2(e)–(g)). However, percolation in three-dimensional network can be predicted using volume fraction, particle size and grain size of the secondary phase present. In all composites, neither of the phases shows abnormally large particle size (Section 3.2) and grain size distribution. Hence, the volume fraction plays a crucial role in deciding the percolation of BCG phase. The volume fractions of composites are listed in Table 1b. According to the symmetric Bruggeman model used for analyzing random composite mixtures, percolation of the second phase starts around 33 vol.%.[16] In the present study, volume fraction of BCG exceeds this percolation limit. Hence, it is likely that the composites have three-dimensional percolating pathways of BCG phase. However, this is to be verified using the conductivity data in the following section.

Table 1b
Volume fractions for the composite samples.

	Nominal mol fraction/mol%		Volume fraction/vol.%	
	CG phase	BCG phase	CG phase[a]	BCG phase[b]
B20CG1450	80	20	65	35
B20CG1550	80	20	65	35
B30CG1550	70	30	52	48

[a] Density of CG phase used in the calculation is 7.24 g cm^{-3}, taken from JCPDS Reference code: 01-075-0162.
[b] Density of BCG phase used in the calculation is 6.36 g cm^{-3}, taken from JCPDS Reference code: 01-082-2373.

3.4. Conductivity measurements

Given the composite nature of the electrolyte, three semi-circles are seen in the impedance spectra, whose visibility depends on the temperature and limitations of the impedance analyzer. These semi-circles can be identified in terms of their frequency range as high frequency (HF), intermediate frequency (IF) and low frequency (LF) semi-circle. Fig. 3(a) shows the impedance spectra of CG201550, BCG151550, B20CG1450, B20CG1550, and B30CG1550 at 200 °C in air and Fig. 3(b) is an enlarged version of the high frequency region of Fig. 3(a). The two overlapping depressed semi circles are visible for all the composites, unlike the single phase systems. The capacitance values extracted from the HF semi-circle at 200 °C for the composites B20CG1550, B20CG1450 and B30CG1550 are 8, 8, and 6 pF cm^{-1}, respectively. Such an order of the capacitance values from the HF semi-circle of the composites, are indicative of the grain response.[8,10] Considering the composite nature of these samples, both the CG and BCG grain can influence the HF semi-circle. However, in this temperature range, the grain conductivity of the BCG phase is significantly higher than CG phase while their permittivity values are of the same order of magnitude.[10,30] The capacitance values extracted from the IF semi-circle for B20CG1550, B20CG1450, and B30CG1550 are 41, 57, and 117 pF cm^{-1}, respectively. These capacitance values are an order of magnitude higher than those associated with the grains of the BCG and CG phase. In addition, these values of capacitance are also an order of magnitude lower than those attributed to the grain boundaries.[8,10,11,30,31] Also, the capacitance associated with these IF semi-circle decreases with an increase in the sintering temperature, which is in contrast to the grain boundary response of the single phase systems.[8,10] This eliminates the possibility of origin of the IF semi-circle from the

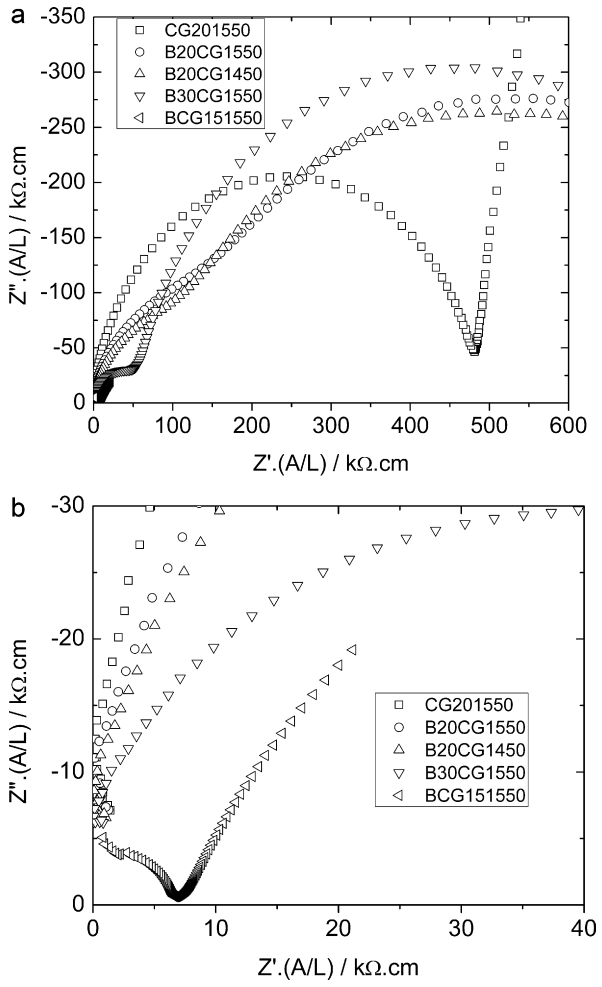

Fig. 3. (a) Impedance spectra in air at 200 °C for CG201550, BCG151550, B20CG1450, B20CG1550 and B30CG1550. The absolute impedance has been multiplied by geometric factor (electrode area/electrolyte thickness) for comparison between samples with different geometric factors. (b) Enlarged view of (a) in high frequency region including impedance spectra in air at 200 °C for CG201550, BCG151550, B20CG1450, B20CG1550 and B30CG1550. The absolute impedance has been multiplied by geometric factor (electrode area/electrolyte thickness) for comparison between samples with different geometric factors.

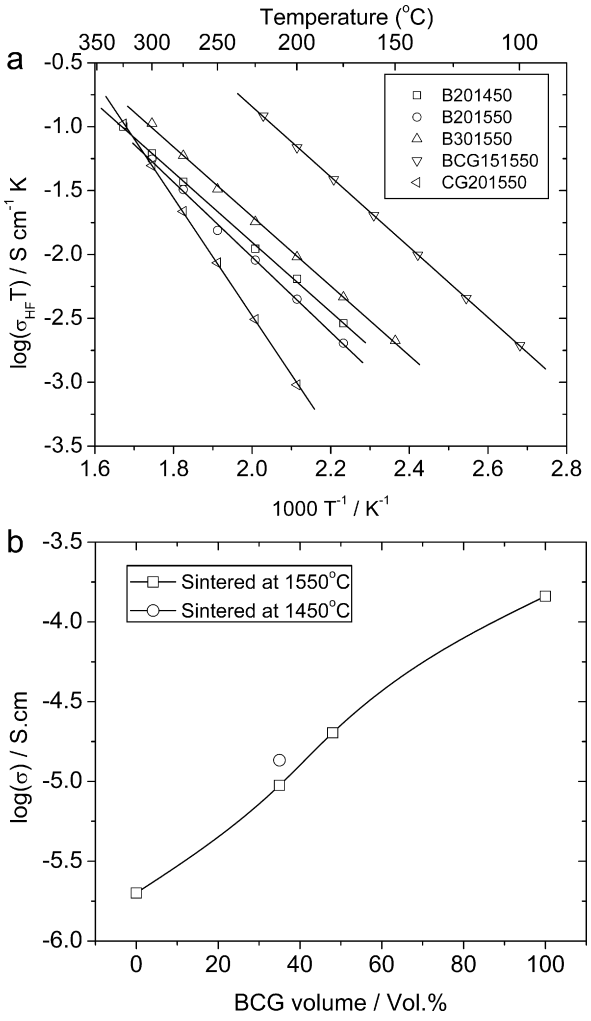

Fig. 4. (a) Temperature dependent high frequency conductivity for B20CG1450, B20CG1550 and B30CG1550. (b) High frequency conductivity as a function of volume fraction of BCG phase at 200 °C.

grain boundary response. However, on the basis of the capacitance values, the IF semi-circle may be attributed to the response of the fraction of small-sized CG grains in the composites.[31]

Fig. 4(a) exhibits the Arrhenius plots for the conductivity values extracted from the HF semi-circle of the impedance spectra for the composites B20CG1450, B20CG1550 and B30CG1550 along with single phase samples CG201550 and BCG151550 for comparison. Above 325 °C, a parallel R-CPE equivalent circuit cannot model the HF semi-circle accurately and hence the resistance values are not extracted at temperatures above this temperature. The activation energy is calculated from the Arrhenius plots using the equation:

$$\sigma = \frac{\sigma_0}{T} \exp\left(\frac{E_a}{kT}\right) \quad (5)$$

where σ is the conductivity, σ_0 is a pre-exponential term, T is the absolute temperature, k is Boltzmann constant and E_a is the activation energy for conduction. The activation energy for the grain conductivity corresponding to the HF semicircle for BCG151550 and CG201550 as well as the composites B20CG1450, B20CG1550 and B30CG1550 is determined from Fig. 4(a) using Eq. (5) and listed in Table 2a. The activation energy for the grain conductivity of BCG151550 is in agreement with the values reported in literature.[10,32,33] For composites, the activation energies for the grain conductivity, corresponding to the HF semi-circle, resembles that of the BCG151550 single phase system. This indicates similarity in the grain charge conduction mechanism in the composites and BCG15, which can be attributed to effective percolation of BCG phase in the composites at the studied compositions.[12] On the other hand, the pre-exponential term for all composites (Table 2b) is significantly lower than that of single phase Gd-doped barium cerates.[32] This can be due to two reasons. First, due blocking of charge conduction by a fraction of CG grains with grain size comparable to BCG grain and secondly, because of lower charge concentration in BCG phase resulting from part of Gd occupying Ba site. This is also reflected by the lower unit cell volume

Table 2a
Activation energy calculated from impedance curves for the HF and IF semi-circles.

Sample	Activation energy/eV	
	HF semi-circle	IF semi-circle
B20CG1550	0.58	0.95
B20CG1450	0.54	1.00
B30CG1550	0.54	0.92
CG201550	0.92	
BCG151550	0.54	
BCG15[a]	0.56	
BCG15[b]	0.56	
BCG15[c]	0.58	

[a] Haile et al.[10]
[b] Bonanos et al.[32]
[c] Stevenson et al.[33]

of BCG phase in the composite samples as indicated in the XRD studies.

The grain conductivity as a function of BCG volume fraction is shown in Fig. 4(b). The curve shown in this figure is guide for eye only. For all composite systems, the grain conductivity increases sharply with the increasing BCG volume fraction. The composites in this work exhibit a 5–10 times increase in the grain conductivity compared to the single phase CG201550. This is a good indicative to the formation of three-dimensional percolating BCG pathways in all composites. Moreover, the grain conductivity for B20CG1450 is higher than B20CG1550. This can be attributed to smaller mean grain size of BCG phase, which is more favorable for the BCG phase percolation to occur.

Fig. 5 exhibits the Arrhenius plots for the conductivity values extracted from the IF semi-circle of the impedance spectra for the composites B20CG1450, B20CG1550 and B30CG1550. The activation energy values are obtained from these plots using Eq. (5) as given in Table 2a. These values are similar to that for Gd-doped ceria systems.[8,30,32] This is in agreement with earlier assignment of IF semi-circle, predominantly, to the fraction of CG phase grains with small grain size, based on the capacitance values.

Fig. 6(a) shows the impedance plots for CG201550, BCG151550, B20CG1550, B20CG1450 and B30CG1550 at 350 °C in air. The HF semi-circle of the impedance spectra is not clearly visible as the relaxation frequency of the grain exceeds the high frequency limit of the impedance analyzer as can be seen in the enlarged view of the HF region in Fig. 6(b). The IF and LF semi-circles are visible as depressed and convoluted semicircle. For the single phase systems, the LF semi-circle is

Table 2b
Pre-exponential factors calculated from impedance curves for the HF semi-circle.

Sample	Pre-exponential term ($\times 10^3$) (S cm^{-1}) K
B20CG1550	7.1
B20CG1450	3.6
B30CG1550	5.5
CG201550	5495.4
BCG1550	45.7

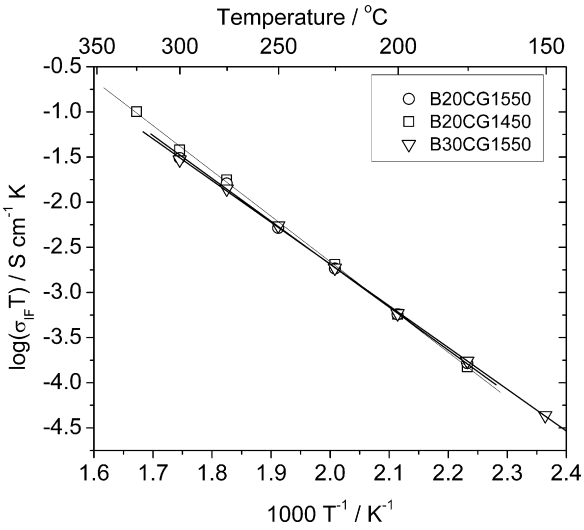

Fig. 5. Temperature dependent intermediate frequency conductivity for B20CG1450, B20CG1550 and B30CG1550.

generally attributed to the charge transfer between electrode and electrolyte.[11,34] However, for the composites, this semi-circle exhibits a change in values with variation in thickness of the pellet, similar to other semi-circles originating from the electrolyte. And thus, this semi-circle can also be said to have origin from the electrolyte only. The capacitance values for this semi-circle for B20CG1550, B20CG1550 and B30CG1550 are 27, 21, and 28 nF cm^{-1}, respectively. This range of capacitance values may be attributed to the grain boundaries or interface between phases.[10] In the temperature range 700–800 °C (not shown), one more semi-circle appears in the impedance spectra. This semi-circle does not show variation with the change in electrolyte thickness. Hence, this semi-circle can be conferred to the electrolyte–electrode interfacial response. The total resistivity of the composite electrolytes is the higher intercept of LF semi-circle with the real axis.

Fig. 7 shows the Arrhenius plot for B20CG1450, B20CG1550 and B30CG1550 for the conductivity values extracted from the LF semi-circle in the temperature range from 350 °C to 800 °C. The plot for B20CG1450 shows a significant change in the slope around 600 °C. Above 600 °C, the activation energy for this sample increases from 1.08 eV to 1.39 eV. This change can arise from the distinct microstructure of B20CG1450. On the other hand, B20CG1550 and B30CG1550 do not show significant change in activation energy (1 eV) over the temperature range of measurement. This indicates similar type of charge transport mechanism in these composites in the temperature range of measurement.

The Arrhenius plots for the total conductivities for CG201550, BCG151550, B20CG1550, B20CG1450 and B30CG1550 samples are shown in Fig. 8. All composite electrolytes exhibit almost a similar dependence of total conductivity on the temperature in air in the studied temperature range. The activation energy for the total conductivity for all the composites is around 0.85 eV, which is similar to that of CG201550. This is in agreement with the activation energy reported for Gd-doped ceria in similar temperature range reported elsewhere.[20] This suggests that the total conductivity

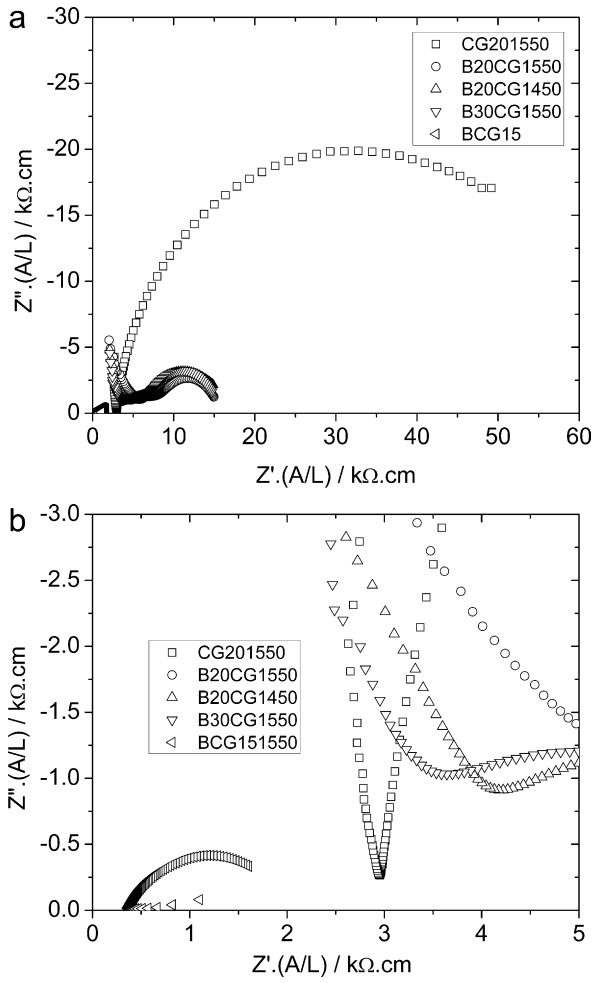

Fig. 6. (a) Impedance spectra in air at 350 °C for CG201550, BCG151550, B20CG1450, B20CG1550 and B30CG1550. The absolute impedance has been multiplied by geometric factor (electrode area/electrolyte thickness) for comparison between samples with different geometric factors. (b) Enlarged view of (a) in high frequency region including impedance spectra in air at 350 °C for CG201550, BCG151550, B20CG1450, B20CG1550 and B30CG1550. The absolute impedance has been multiplied by geometric factor (electrode area/electrolyte thickness) for comparison between samples with different geometric factors.

of these composites is controlled by the CG phase in this temperature range. The total conductivity at 800 °C for B20CG1550, B20CG1450 and B30CG1550 are 2.8×10^{-2}, 3.4×10^{-2} and 2.6×10^{-2} S cm^{-1}, respectively. The total conductivity values of the composite electrolytes are lower than that of CG201550. This can be attributed to the presence of BCG phase which has comparatively a lower charge concentration and thus resulting into lower conductivity.

3.5. Fuel cell test

Fig. 9 shows the cell voltage and power density as a function of current density at 800 °C for SOFCs based on $Ce_{0.8}Gd_{0.2}O_{1.9}$ and composite electrolytes. The OCV and peak power density for CG201550 are 0.73 V and 20 mW cm^{-2}, respectively. This OCV is lower than the theoretically predicted OCV owing to the electronic conductivity in doped ceria and choice of elec-

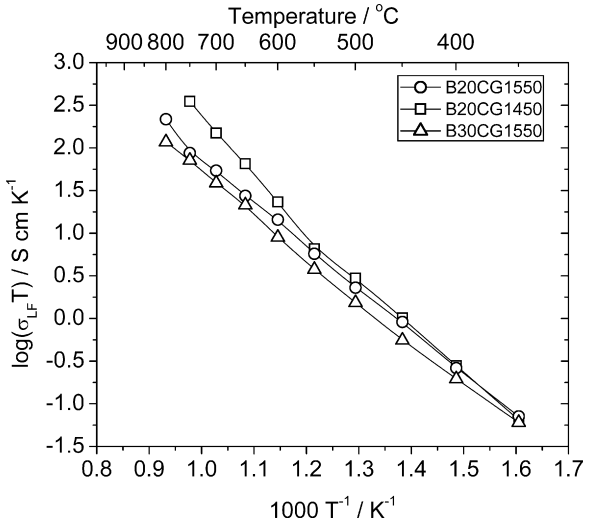

Fig. 7. Temperature dependent low frequency conductivity for B20CG1450, B20CG1550 and B30CG1550.

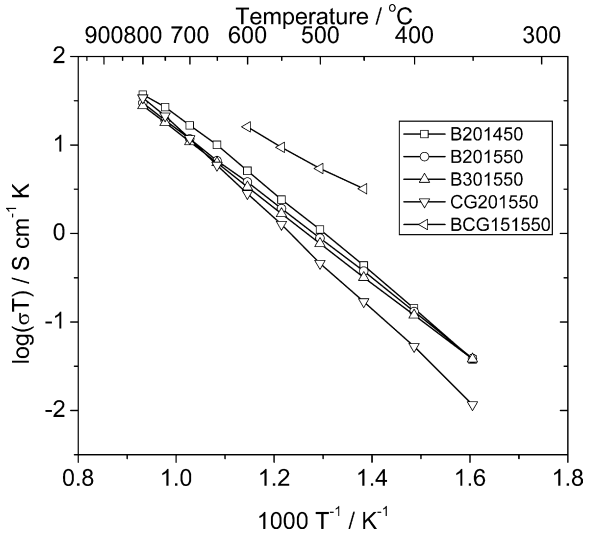

Fig. 8. Arrhenius plots of total conductivity for CG201550, BCG151550, B20CG1450, B20CG1550 and B30CG1550.

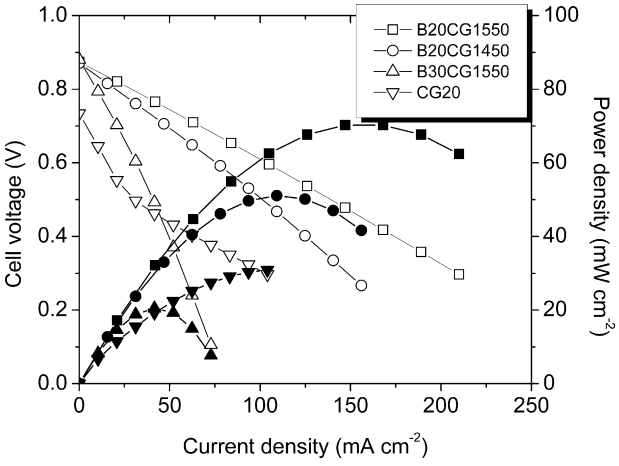

Fig. 9. The cell voltage and power density as a function of current density for CG201550, B20CG1450, B20CG1550 and B20CG1550. Open and close symbols represent cell voltage and power density, respectively.

trode materials.[35] The non-linear decrease in the cell voltage with an increase in current density originates from activation polarization.

In general, all SOFC constructed with composite electrolyte exhibit a higher OCV than CG201550. The OCV of SOFCs constructed using B20CG1550, B20CG1450 and B30CG1550 are 0.87, 0.87 and 0.89 V, respectively. This increase in OCV is partly due to the blocking of electronic current by BCG phase.[36] The similarity in the OCVs for SOFCs constructed using composite electrolytes B20CG1550 and B20CG1450 indicates that the blocking effect by BCG phase is not affected much by its grain size. The OCV for SOFC using B30CG1550 is slightly higher than rest of the composite electrolytes. This can be attributed to higher mol fraction of BCG phase present. The SOFCs with composite electrolytes show a linear drop in cell voltage with an increase in current density. This is due to Ohmic polarization arising from thick pellets as electrolytes used in this study. The slope of *I–V* plot corresponds to the Ohmic resistance predominantly from the composite electrolyte. The composite electrolytes B20CG1550 and B20CG1450 show a significant increase in the total conductivity in fuel cell atmosphere compared to air. In contrast, B30CG1550 does not show such an increase. This can be attributed to higher proton conductivity in BCG phase present in B20CG1450 and B20CG1550 than B30CG1550.The peak power densities for B20CG1550, B20CG1450 and B30CG1550 are 70, 50 and 30 mW cm^{-2}, respectively. The obtained low power densities are due to thick electrolytes used in the study. These power densities can be further improved by thinner electrolytes with suitable electrode materials.

4. Conclusion

In this work, Gd-doped ceria and Gd-doped barium cerate composites were synthesized through the citrate route. The formation of two phase microstructure was confirmed through X-ray diffraction and electron microscopy. It was revealed that the presence of Gd-doped barium cerate phase arrested the grain growth of Gd-doped ceria phase. The three distinct semi-circles associated with the electrolyte were observed in the impedance spectra of the composite electrolytes, unlike the single phase systems. On the basis of capacitance and the activation energy values extracted from the temperature dependent conductivity, the high frequency and intermediate frequency semi-circles were attributed predominantly to the Gd-doped barium cerate and Gd-doped ceria phase, respectively. The low frequency semi-circle was attributed to the grain boundary and interfacial response. The activation energy associated with the conductivity values extracted from the low frequency semi-circle was found to vary significantly with microstructure. The SOFCs based on composite electrolyte showed appreciable improvement in open circuit voltage over those based on 20% Gd-doped ceria as electrolyte. Further improvement in the performance can be made on the basis of understanding developed by this work on the microstructure–conductivity correlation.

Acknowledgement

The authors would like to thank NMRL, Additional Ambernath for funding this work.

References

1. Arachi Y, Sakai H, Yamamoto O, Takeda Y, Imanishai N. Electrical conductivity of the ZrO_2–Ln_2O_3 (Ln = lanthanides) system. *Solid State Ionics* 1999;**121**:133–9.
2. Eguchi K, Setoguchi T, Inoue T, Arai H. Electrical properties of ceria-based oxides and their application to solid oxide fuel cells. *Solid State Ionics* 1992;**52**:165–72.
3. Kudo T, Obayashi H. Mixed electrical conduction in the flourite-type $Ce_{1-x}Gd_xO_{2-x/2}$. *J Electrochem Soc* 1976;**123**:415–9.
4. Iwahara H, Uchida H, Ono K, Ogaki K. Proton conduction in sintered oxides based on $BaCeO_3$. *J Electrochem Soc* 1988;**135**:529–33.
5. Bonanos N. Transport study of the solid electrolyte $BaCe_{0.9}Gd_{0.1}O_{2.95}$ at high temperatures. *J Phys Chem Solids* 1993;**54**:867–70.
6. Hirabayashi D, Tomita A, Hibino T, Nagao M, Sano M. Design of a reduction-resistant $Ce_{0.8}Sm_{0.2}O_{1.9}$ electrolyte through growth of a thin $BaCe_{1-x}Sm_xO_{3-\delta}$ layer over electrolyte surface. *Electrochem Solid State* 2004;**7**:A318–20.
7. Zhu B, Liu X, Schober T. Novel hybrid conductors based on doped ceria and BCY20 for ITSOFC applications. *Electrochem Comm* 2004;**6**:378–83.
8. Christie GM, Van Berkel EPF. Microstructure ionic conductivity relationships in ceria–gadolinia electrolytes. *Solid State Ionics* 1996;**83**:17–27.
9. Zhan Z, Wen TL, Tu H, Lu ZY. AC Impedance investigation of samarium-doped ceria. *J Electrochem Soc* 2001;**148**:A427–32.
10. Haile SM, West DL, Campbell J. The role of microstructure and processing on the proton conducting properties of gadolinium-doped barium cerate. *J Mater Res* 1998;**13**:1576–95.
11. Coors WG, Readey DW. Proton conductivity measurements in yttrium barium cerate by impedance spectroscopy. *J Am Ceram Soc* 2002;**85**:2637–40.
12. M'Peko JC, Spavieri Jr DL, da Silva CL, Fortulan CA, de Souza DPF, de Souza MF. Electrical properties of zirconia–alumina composites. *Solid State Ionics* 2003;**156**:59–69.
13. Muccillo ENS, Kleitz M. Ionic conductivity of fully stabilized ZrO_2: MgO and blocking effects. *J Eur Ceram Soc* 1995;**15**:51–5.
14. Fonseca FC, Muccillo R. Impedance spectroscopy analysis of percolation in (yttria-stabilized zirconia)–yttria ceramic composites. *Solid State Ionics* 2004;**166**:157–65.
15. Zhang T, Zeng Z, Huang H, Hing P, Kilner J. Effect of alumina addition on the electrical and mechanical properties of $Ce_{0.8}Gd_{0.2}O_{2-\delta}$ceramics. *Mater Lett* 2002;**57**:124–9.
16. Bonanos N, Steele BCH, Butler EP. In: Barsoukov E, Macdonald JR, editors. *Characterization of Materials in Impedance Spectroscopy Theory Experiments and Applications*. John Wiley & Sons, Inc.; 2005. p. 205–63.
17. Lee DW, Won JH, Shim KB. Low temperature synthesis of $BaCeO_3$ nano powders by the citrate process. *Mater Lett* 2003;**57**:3346–51.
18. Udawatte CP, Kakihana M, Yoshimura M. Low temperature synthesis of pure $SrSnO_3$ and the $(Ba_xSr_{1-x})SnO_3$ solid solution by the polymerized complex method. *Solid State Ionics* 2000;**128**:217–26.
19. Flint SD, Slade RCT. Comparison of calcium-doped barium cerate solid electrolytes prepared by different routes. *Solid State Ionics* 1995;**77**:215–21.
20. Torrens RS, Sammes NM, Tompsett GA. Characterization of $(CeO_2)_{0.8}(GdO_{1.5})_{0.2}$ synthesized using various techniques. *Solid State Ionics* 1998;**111**:9–15.
21. Birkenstock J, Fischer RX, Messner T. *BRASS 2: The Bremen Rietveld Analysis and Structure Suite*. University of Bremen; 2004. www.brass.uni-bremen.de.
22. Makino Y, Uchida S. In: Adachi G, Imanaka N, Kang ZC, editors. *Binary Rare Earth Oxides*. Kluwer Academic Publishers; 2004. p. 95.
23. Knight KS, Bonanos N. Space group and lattice constants for barium cerate and minor corrections to the crystal structures of $BaCe_{0.9}Y_{0.1}O_{2.95}$ and $BaCe_{0.9}Gd_{0.1}O_{2.95}$. *J Mater Chem* 1994;**4**:899–901.

24. Butee S, Kulkarni A, Prakash O, Aiyar R, George S, Sebastian M. High Q microwave dielectric ceramics in $(Ni_{1-x}\ Zn_x)Nb_2O_6$ system. *J Am Ceram Soc* 2009;**92**:1047–53.
25. Orazem ME, Tribollet B. *Electrochemical Impedance Spectroscopy*. John Wiley & Sons, Inc.; 2008. pp. 129–152.
26. Charpentier P, Fragnaud P, Schleich DM, Gehain E. Preparation of thin film SOFCs working at reduced temperature. *Solid State Ionics* 2000;**135**:373–80.
27. Bevan DJM, Summerville E. In: Gschneider KA, Eyring L, editors. *Handbook on the Physics and Chemistry on Rare Earth's, vol. 3*. Amsterdam: North-Holland Publishing Company; 1979. p. 423.
28. Taniguchi N, Hatoh K, Niikura J, Gamo T, Iwahara H. Proton conductive properties of gadolinium-doped barium cerates at high temperatures. *Solid State Ionics* 1992;**53–56**:998–1003 (part 2).
29. Wu J, Li LP, Espinosa WTP, Haile SM. Defect chemistry and transport properties of $Ba_xCe_{0.85}M_{0.15}O_{3-\delta}$. *J Mater Res* 2004;**19**:2366–76.
30. Duncan H, Lasia A. Influence of the electrode nature on conductivity measurements of gadolinia-doped ceria. *Solid State Ionics* 2005;**176**: 1429–37.
31. Fletcher JG, West AR, Irvine JTS. The AC impedance response of the physical interface between yttria-stabilized zirconia and $YBa_2Cu_3O_{7-x}$. *J Electrochem Soc* 1995;**142**:2650–4.
32. Bonanos N, Ellis B, Knight KS, Mahmood MN. Ionic conductivity of gadolinium-doped barium cerate perovskites. *Solid State Ionics* 1989;**35**:179–88.
33. Stevenson DA, Jiang N, Buchanan RM, Henn FEG. Characterization of Gd, Yb and Nd doped barium cerates as proton conductors. *Solid State Ionics* 1993;**62**:279–85.
34. Coll DP, Lopez DM, Numez P, Pinol S, Frade JR. Grain boundary conductivity of $Ce_{0.8}Ln_{0.2}O_{2-(}$ceramics (Ln = Y, La, Gd, Sm) with and without Co-doping. *Electrochim Acta* 2006;**51**:6463–9.
35. Zha S, Xia C, Meng G. Effect of Gd (Sm) doping on properties of ceria electrolyte for solid oxide fuel cells. *J Power Sources* 2003;**115**:44–8.
36. Mishima Y, Mitsuyasu H, Ohtaki M, Eguchi K. Solid oxide fuel cell with composite electrolyte consisting of samaria-doped ceria and yttria-stabilized zirconia. *J Electrochem Soc* 1998;**145**:1004–7.